The Journal of Engineering Geology, Vol.14, No.1, March, 2004, pp. 29-46

스펙트럼 분석을 응용한 단일 균열 규모확장과 투수계수 산정

채병곤*
한국지질자원연구원 지질환경재해연구부

Scaling up of single fracture using a spectral analysis and computation of its permeability coefficient

Byung-Gon Chae*
Korea Inst. Geoscience and Mineral Res.

균열을 따른 지하수 유동은 균열 기하양상에 의해 속도와 유동형태가 결정되므로, 암반 내 지하수 유동특성 해석 시 유동경로 역할을 하는 균열의 기하양상을 정확하게 파악하는 것은 중요하다. 그러나, 실제 현장규모에서는 노두의 불연속적 분포와 지표 하 정보의 연속적 획득이 불가능하기 때문에 전체적인 균열 정보를 얻기 어렵다. 따라서, 해석대상 균열 전체양상을 표현할 수 있는 방법의 개발이 요구된다.

이 연구는 퓨리에 변환을 토대로 해석대상 균열의 전체 기하양상을 파악하는 방법을 개발하고자 새로운 접근을 시도하였다. 시추코아로 부터 해석대상 균열을 따라 시료를 채취한 후, 각 시료별로 퓨리에 변환을 통해 거칠기 구성성분 중 영향력이 큰 성분을 선택하였다. 그리고, 선정된 성분들을 평균하여 평균 스펙트럼을 구하였다. 평균 스펙트럼은 각 시료의 모든 성분을 포함하고 있으므로, 해석 대상 균열의 거칠기 성분 중 대표성분을 나타낸다. Low pass filtering을 수행한 후, 퓨리에 역변환을 실시하여 평균화 된 전체 균열의 거칠기 형상을 재현하였다. 재현된 거칠기 형상 또한 각 시료의 전체 기하특성을 포함하는 해석대상 지표하 균열의 대표적 거칠기 양상을 나타내는 것이다. 또한, 이는 규모확장을 통한 균열 전체의 거칠기 양상을 의미하는 것이다.

해석대상 균열을 따른 투수계수 특성을 파악하기 위해 재현된 거칠기 양상을 바탕으로 균열모델을 구성하였다. 투수계수는 균열 기하특성을 최대한 반영하여 정확한 투수계수를 구할 수 있는 균질화 해석법을 통해 산정하였다. 해석결과는 10^{-4} and 10^{-3} cm/sec 범위의 투수계수 분포를 보이는데, 이는 큰 규모의 균열을 따른 투수계수 값이라 할 수 있다. 이러한 시도는 전술한 바와 같이 제한된 단속적 균열정보를 이용해 해석대상의 균열 전체에 대한 기하양상은 물론 투수계수를 산정할 수 있는 방법이 될 것이다.

주요어: 거칠기, 퓨리에 변환, 규모확장, 투수계수, 균질화 해석법

It is important to identify geometries of fracture that act as a conduit of fluid flow for characterization of groundwater flow in fractured rock. Fracture geometries control hydraulic conductivity and stream lines in a rock mass. However, we have difficulties to acquire whole geometric data of fractures in a field scale because of discontinuous distribution of outcrops and impossibility of continuous collecting of subsurface

* Corresponding author : bgchae@kigam.re.kr

data. Therefore, it is needed to develop a method to describe whole feature of a target fracture geometry.

This study suggests a new approach to develop a method to characterize on the whole feature of a target fracture geometry based on the Fourier transform. After sampling of specimens along a target fracture from borehole cores, effective frequencies among roughness components were selected by the Fourier transform on each specimen. Then, the selected effective frequencies were averaged on each frequency. Because the averaged spectrum includes all the frequency profiles of each specimen, it shows the representative components of the fracture roughness of the target fracture. The inverse Fourier transform is conducted to reconstruct an averaged whole roughness feature after low pass filtering. The reconstructed roughness feature also shows the representative roughness of the target subsurface fracture including the geometrical characteristics of each specimen. It also means that overall roughness feature by scaling up of a fracture.

In order to identify the characteristics of permeability coefficients along the target fracture, fracture models were constructed based on the reconstructed roughness feature. The computation of permeability coefficient was performed by the homogenization analysis that can calculate accurate permeability coefficients with full consideration of fracture geometry. The results show a range between 10^{-4} and 10^{-3} cm/sec, indicating reasonable values of permeability coefficient along a large fracture. This approach will be effectively applied to the analysis of permeability characteristics along a large fracture as well as identification of the whole feature of a fracture in a field scale.

Key words: Roughness, Fourier transform, Scaling up, Permeability, Homogenization analysis method

INTRODUCTION

In general, fracture acts as a conduit of fluid flow in a fractured rock. Fracture geometries, therefore, affect permeability coefficients and stream lines in rock masses. Therefore, it is necessary to characterize geometric feature of the whole conduit of fluid flow.

There have been many researches related to the measurement methods of fracture roughness and aperture. In case of roughness, most of the measurements have been conducted with a profilometer (ISRM, 1978; Brown and Scholz, 1985; Keller and Bonner, 1985; Durham and Bonner, 1993; Kulatilake et al., 1995; Lee et al., 1990; Power and Durham, 1997; Lespinasse and Sausse, 2000; Plouraboue et al., 2000; Develi et al., 2001). Several researchers developed a graphic techniques to measure fracture roughness (Krohn and Thompson, 1986; Jesselle et al., 1995; Maerz et al., 1990). In recent, several equipments using laser beam have been used for the roughness measurement (Huang et al. 1988; Brown, 1995; Chae et al., 2003b).

For observation of aperture, a resin, epoxy and molten Wood's metal were injected into a fracture. After consolidation of those materials, fracture was sliced in several direction to measure aperture distribution (Gale, 1987; Gentier et al., 1989; Hakami and Stephansson, 1993; Hakami and Barton, 1990; Hakami, 1992; Persoff and Pruess, 1995). Besides the above methods, X-ray tomography (Adler and Thovert, 1999; Ichikawa et al., 2001), mercury intrusion porosimetry (Tsang and Hale, 1988), helium-water drive method (Gash, 1991), light transmission method (Glass et al., 1995; Persoff and Pruess, 1995; Brown et al., 1998), and a confocal laser scanning microscope (Chae et al., 2003a) have been used to measure the apertures along fractures.

The measured geometry data should be treated appropriately to identify geometric features such as aperture and roughness effectively. The data must also be representative ones of the whole feature of the geometry. Therefore, it is important to select a range of measurement and to determine a threshold of scale effect for an accurate analysis. Most of the methods mentioned above, however, are performed in a laboratory scale. In that case, local effect of a fracture

might be emphasized than that of the whole fracture in a field scale. However, it is very difficult to acquire the whole data of fractures in a field scale because of discontinuous distribution of outcrops and impossibility of continuous acquisition of subsurface data. Therefore, it is needed to develop a method to describe the whole feature of a target fracture geometry.

This study suggests a new approach to develop a method to characterize on the whole feature of a target fracture geometry based on the Fourier transform that has been usually applied for analysis of fracture roughness. After sampling of fracture along a target fracture from a drilled core, effective frequencies among roughness components were selected by the Fourier transform on each specimen. The selected effective frequencies were averaged, and then, they were treated by the inverse Fourier transform to reconstruct the representative roughness feature of the target fracture in a field scale. In order to identify the characteristics of permeability coefficients along the target fracture, fracture models were constructed based on the reconstructed roughness feature. The computation of permeability coefficient was performed by the homogenization analysis that can calculate accurate permeability coefficients with full consideration of fracture geometry. This approach will be effectively applied to the analysis of permeability characteristics along a large fracture as well as identification of whole fracture feature in a field scale.

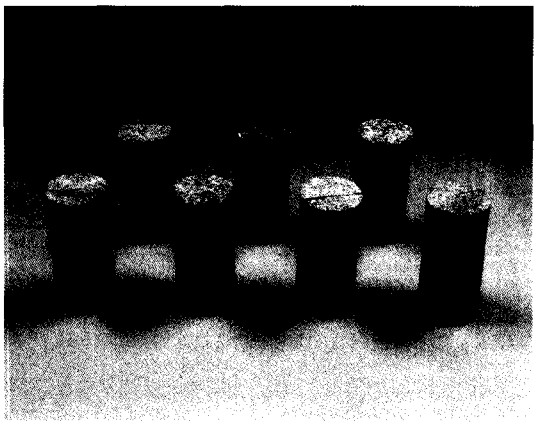

Fig. 1. The core specimens collected along a vertical fracture.

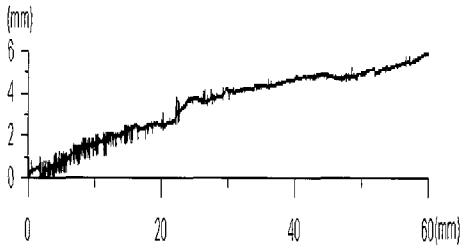

Fig. 2. An example of fracture roughness measured with a confocal laser scanning microscope (left part of GRA).

ROCK SPECIMENS

The specimens are composed of the Jurassic coarse-grained granite, which were collected from the drilled cores at Iksan area, the mid-western part of Korea. Among the cores six specimens that contain a single, fresh fracture parallel or subparallel to the long axis of the core were studied in detail. The size is 5.5x11.0cm (Fig. 1). They were designated as GRA, GRB, ..., GRF. The rock specimens have the composition of a typical granite, containing mainly quartz, feldspar, biotite and some mafic minerals.

Roughness patterns of the specimens were measured with a confocal laser scanning microscope(Fig. 2). The wavelength and the highest resolution in z direction of the laser beam are 488㎚ and 0.05㎛, respectively. Therefore, it can acquire roughness data with very high resolution in a digital format(Chae et al., 2003b).

FOURIER TRANSFORM OF THE FRACTURE ROUGHNESS

Fourier series and Fourier transform

The Fourier spectral analysis was performed to recognize influential components of the measured fracture roughness. It can analyze complicated components into simple frequency components representing the magnitudes of the analyzed frequencies. Therefore, it is possible to identify the whole composition of frequency by the Fourier spectral analysis. If a certain frequency of roughness data has larger magnitude than those of others, the frequency component contributes stronger to the composition of the whole roughness pattern than other frequencies(Brown, 1987; Durham and Bonner, 1993; Plouraboue et al., 2000). Based on the results of the Fourier spectral analysis, the most effective frequency or the dominant frequencies can be recognized among the roughness data. In this study, one period of the signal was assigned as the whole length of the scanning line of roughness, that is, 60 mm in length.

A function f defined on (-L/2, L/2) can be written in the discrete Fourier series if f is square integrable and a set of discrete values $\{fm\}$ is given as

$$f(x) \cong \{f_m\} = \sum_{n=0}^{N-1} \hat{f}_n * exp(ik_n m\Delta x) \quad (1)$$

where L is the length of the domain, Δx the sampling interval, N the number of sampling data, $k_n=2\pi n/L$ the angular frequency, and

$$\hat{f}_n * = \frac{1}{N}\sum_{m=0}^{N-1} f_n \; exp(-ik_n m\Delta x) \quad (2)$$

are the Fourier coefficients. Note that f^* implies the complex conjugate of f. Then the Fourier spectrum $|\hat{f}_n|$, the power spectrum

$$G(k_n) = \frac{1}{L} |\hat{f}_n|^2 \quad (3)$$

and the phase spectrum

$$\phi_n = tan^{-1}\left(-\frac{Im(\hat{f}_n)}{Re(\hat{f}_n)}\right) \quad (4)$$

can be easily calculated corresponding to each frequency k_n (n=0,1,...,N-1). Note Re(f) is the real part of f, and Im(f) is its imaginary part.

Recall that the mean value is $\bar{f} = \hat{f}_0$, and the mean power is calculated by

$$\frac{1}{N}\sum_{m=0}^{N-1} f_m^2 = \frac{1}{N}\sum_{n=0}^{N-1} |\hat{f}_n|^2 \text{ (parseval equation)} \quad (5)$$

Then the variance σ^2 is

$$\sigma^2 = \frac{1}{N}\sum_{m=0}^{N-1} f_m^2 - \bar{f}^2 = \frac{1}{N}\sum_{n=1}^{N-1} \hat{f}_n^2 \quad (6)$$

Since the autocovariance R_j is given as

$$R_j = \frac{1}{N} \; f_m \; f_{m+j'} \quad (7)$$

its Fourier coefficients can be calculated as

$$\begin{aligned} R_n * &= \left(\sum_{j=0}^{N-1} Rj\right)* \\ &= \frac{1}{N}\sum_{j=0}^{N-1} R_j exp(-ik_n j\Delta x) \\ &= |\hat{f}_n|^2 \end{aligned} \quad (8)$$

so the power spectrum can be easily calculated by Eqs. (7) and (8). Note that the inverse relation of Eq. (8) is given by the inverse Fourier transformation:

$$R_j = \frac{1}{N}\sum_{n=0}^{N-1} |\hat{f}_n| \, exp(ik_n j\Delta x) \quad (9)$$

If the Fourier spectral analysis is applied to the measured data of roughness, it is possible to identify the characteristics of dominant undulations corresponding to these frequencies. Furthermore, if the dominant phase spectra are known, it is easy to reconstruct the original function f excluding the noise data.

The number of roughness data measured by the confocal laser scanning microscope is 24,000, and in order to apply the fast Fourier transform (FFT), 8,768 data with zero values are added, so the total data number is 32,768 (=215). Because the sampling interval Δx is 0.0025 mm, the frequency f_k can be represented as

$$f_k = \frac{k}{N\Delta x} = \frac{k}{32768 \times 0.0025} = \frac{k}{82} \quad (10)$$

Next the continuous forms of Eqs. (1) and (2) are considered. Let $\Delta x \to 0$ and $L \to \infty$, then the following Fourier and inverse Fourier transforms can be introduced:

$$f_k = \frac{1}{\sqrt{2\pi}}\int_{\infty}^{-\infty} dk\,\hat{f}(k)exp(ikx)$$
$$= < f^*(k), \phi(k,x) >_k \quad (11)$$
$$\equiv F^{-1}(f)$$

$$\hat{f}_k = \frac{1}{\sqrt{2\pi}}\int_{\infty}^{-\infty} dx\, f(x)exp(-ikx)$$
$$= < f(x), \phi^*(k,x) >_x \quad (12)$$
$$\equiv F(f)$$

where $\phi(k,x) = exp(ikx)/\sqrt{2\pi}$ provides the Fourier basis.

Now the continuous form of the autocovariance R(ξ) corresponding to Eq. (7) is given by

$$R(\xi) \equiv < f(x)f(x+\xi) >$$
$$= \lim_{L\to\infty}\frac{1}{L}\int_{-L/2}^{L/2} f(x)f(x+\xi)dx \quad (13)$$

The mean power is calculated by using the Fourier inverse transformation as

$$R(0) \equiv < f(x)^2 >$$
$$= \lim_{L\to\infty}\frac{1}{L}\int_{-L/2}^{L/2} f(x)^2 dx$$
$$= \lim_{L\to\infty}\frac{2\pi}{L}\int_{-L/2}^{L/2} dk\hat{f}(k)exp(kx)$$
$$\frac{1}{\sqrt{2\pi}}\int_{-\infty}^{\infty} dk f(k')exp(k'x)$$
$$= \lim_{L\to\infty}\frac{2\pi}{L}\int_{-\infty}^{\infty} dk\,\hat{f}(k)f(-k)$$
$$= 2\pi\int_{-\infty}^{\infty} G(k)dk$$

Here the power spectrum $G(k)$ is defined by

$$G(k) = \lim_{L\to\infty}\frac{|\hat{f}(k)|^2}{L} \quad (14)$$

and the following δ-function identity is used:

$$\delta(x) = \frac{1}{2\pi}\int_{-\infty}^{\infty} exp(ikx)dx$$

By introducing the Fourier transform to Eq. (13) the spectral representation of auto-correlation function $R(\xi)$ known as the Wiener-Khintchine's theorem is obtained:

$$G(k) = F(R(\xi)),\ R(\xi) = F^{-1}(G(k)) \quad (15)$$

This is because

$$FR(0) \equiv < F(x)^2 > = \lim_{L\to\infty}\frac{1}{L}\int_{-L/2}^{L/2} f(x)^2 dx$$

$$F(R(\xi) = \frac{1}{\sqrt{2\pi}}\int_{-\infty}^{\infty} R(\xi)exp(-ikx)dk$$
$$= \frac{1}{\sqrt{2\pi}} < f(x)\int_{-\infty}^{\infty} f(x+\xi)$$
$$exp(-ik(x+\xi)d\xi exp(ikx) >$$
$$= < f(x)exp(ikx) > \hat{f}^*(k)$$
$$= \lim_{L\to\infty}\frac{1}{L}\int_{-L/2}^{L/2} f(x)exp(ikx)dx f(k)$$
$$= \lim_{L\to\infty}\frac{1}{L}\hat{f}^*(k)f(k)$$
$$= G(k)$$

The convolution of functions f and g is defined by

$$(f*g)(x) = \int_{-\infty}^{\infty} d\xi f(\xi)g(x-\xi) \quad (16)$$

The Fourier transforms of the convolution is given by

$$F(f*g) = \sqrt{2\pi}F(f)F(g)$$
$$= \sqrt{2\pi}\ \hat{f}\ \cdot\hat{g}$$
$$F^{-1}(\hat{f}\cdot\hat{g}) = \frac{1}{2\pi}F^{-1}(f)F^{-1}(g) \quad (17)$$
$$= \frac{1}{2\pi}f*g$$

Based on the above procedure, spectral analysis was conducted to identify the components of roughness and to select effective frequency among all the frequency components (Fig. 3).

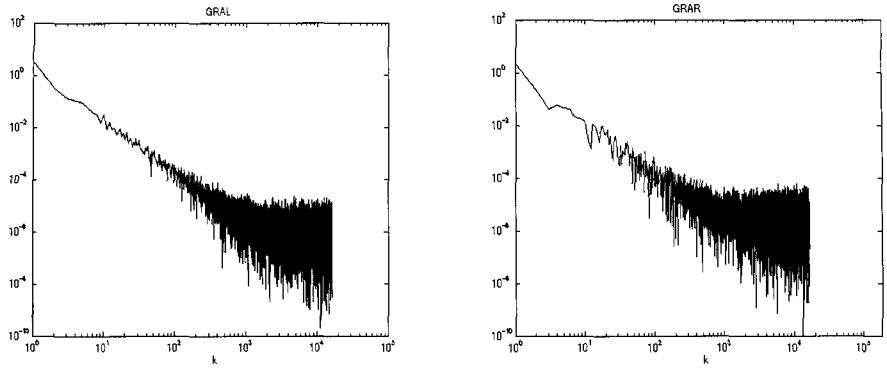

(a) GRA

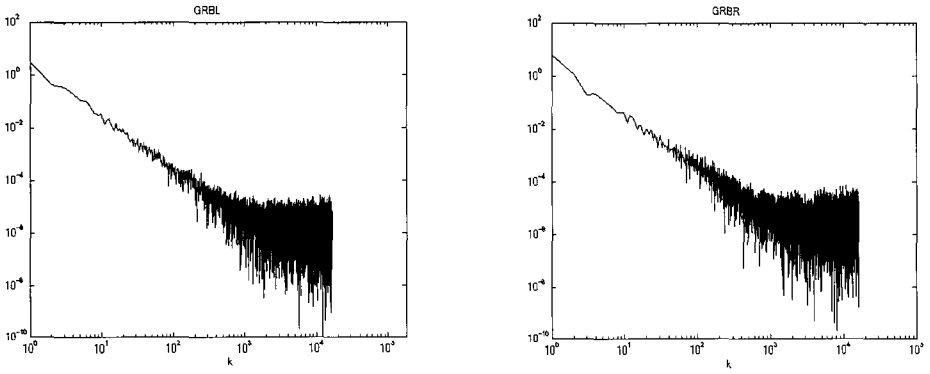

(b) GRB

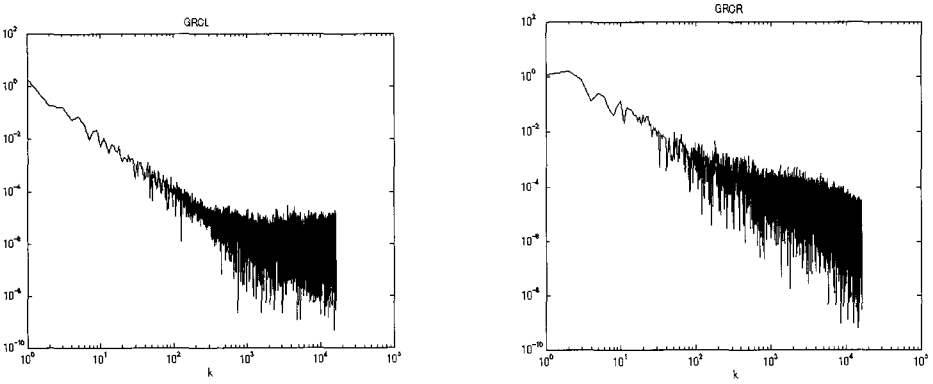

(c) GRC

Fig. 3. Result of spectral analysis using the fast Fourier transform. 'L' of each specimen title meas left part, while 'R' means right part of a specimen.

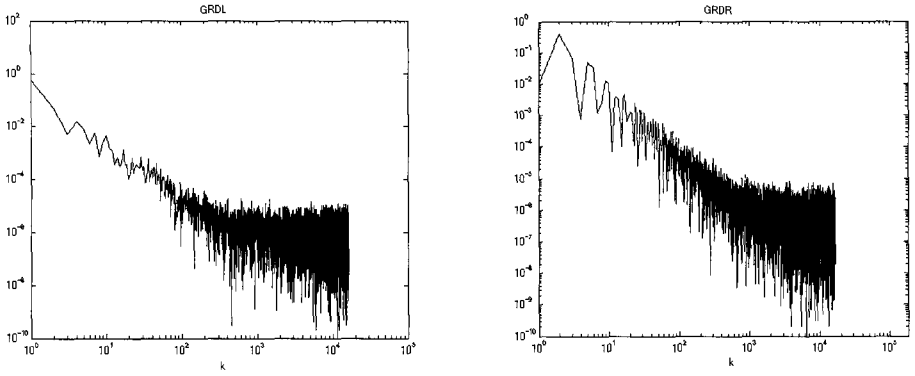

(d) GRD

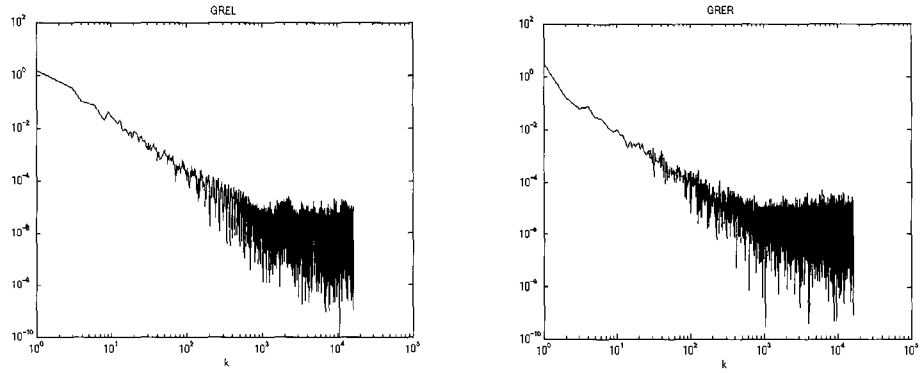

(e) GRE

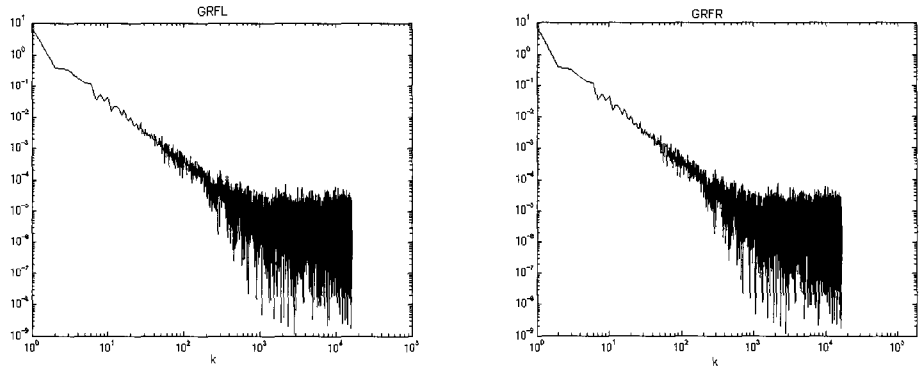

(f) GRF

Fig. 3. Continued.

Smoothing of the spectrum

i) Data window

For data smoothing a uniform interval b is set, so that the average value of sample data in this interval b can be calculated. The total smoothed data can be obtained by moving the central point of b and by averaging in the domain successively. This method is called the moving average method (Ohsaki, 1976). Let $w(x)$ be a 'weight function' to make f smooth $w(x)$ is called the 'data window'). The smoothed f by the above moving average method under the weight $w(x)$ can be written as

$$\bar{f}(x) = \int_{-\infty}^{\infty} d\xi f(x) w(x-\xi) = f(x) * w(x) \tag{18}$$

Recalling Eq. (18) its Fourier transform is given by

$$F(f*w) = \sqrt{2\pi} F(f) F(w) \tag{19}$$

where the Fourier transform of w is calculated as

$$W(k) = F(w) = \frac{1}{\sqrt{2\pi}} \int_{-\infty}^{\infty} dx w(x) exp(-ikx) \tag{20}$$

For example if considering the rectangular pulse such that

$$w(x) = \begin{cases} \frac{1}{b}, & |x| \leq \frac{b}{2} \\ 0, & |x| > \frac{b}{2} \end{cases}$$

its Fourier transform is given by

$$W(k) = \frac{1}{\sqrt{2\pi} b} \int_{-b/2}^{b/2} dx exp(-ikx) = \frac{1}{\sqrt{2\pi} kb/2} sin(kb/2)$$

ii) Spectral window

Similar to the data window w(x), the spectral window $W(k)$ can be introduced as:

$$\bar{G}(k) = \int_{-\infty}^{\infty} d\kappa G(\kappa) W(k-\kappa) = G(k) * W(k) \tag{21}$$

where $W(k)$ must be satisfied the properties

$$\int_{-\infty}^{\infty} W(k) dk = 1, \quad W(k) = W(-k)$$

This $W(k)$ works as a band-pass filter, and the band width b can be introduced by the variance σ^2 by

$$b = \frac{1}{\sigma^2} \tag{22}$$

Among the spectral windows such as rectangular pulse, rectangular window, Barlett window and Parzen window that are mainly used in the spectral domain, this study also used Parzen window for smoothing of the spectrum, because it has a smooth peak at the center and a very narrow side lobe.

$$W(f) = \frac{3}{4} u \left(\frac{sin(uk/4)}{uk/4} \right)^4 \tag{23}$$

The dispersion can be calculated as σ^2 = 280u / 151.

Since the band width b (the unit is cpmm cycle per mm] in this study) is always inversely proportioned to the given constant u (unit; mm), the band width becomes wide when the constant u is small. Therefore, the data under smoothing with narrow b become smoother.

iii) Lag window

Recall the spectral representation of the autocorrelation function given by Eq. (15):

$$G(k) = F(R(\xi)), \quad R(\xi) = F^{-1}(G(k))$$

Let us introduce this for the smoothed relation

$$R(\xi)=\frac{1}{\sqrt{2\pi}}\int_{-\infty}^{\infty}G(k)exp(-ik\xi)$$
$$=\frac{1}{\sqrt{2\pi}}\int_{-\infty}^{\infty}dk$$
$$\cdot\left[\int_{-\infty}^{\infty}G(k)\,W(k-k)dk\right]exp(-ik\xi)$$
$$=F^{-1}(G^{*}\,W)$$
$$=\sqrt{2\pi}F^{-1}(G)F^{-1}(W)$$
$$=\sqrt{2\pi}R(\xi)w(\xi)$$

Calculating $w(x)$ yields the followings:

$$w(x)=$$

$$\begin{cases}1-6(\frac{\xi}{u})^2+6(\frac{|\xi|}{u})^3, & |\xi|\leqq\frac{u}{2}\\ 2(1-\frac{|\xi|}{u})^3, & \frac{u}{2}\leqq|\xi|\leqq u\\ 0, & |\xi|>u\end{cases}\quad(24)$$

Based on the above smoothing theory, noises of the analyzed roughness spectra were reduced by the Parzen window (Fig. 4).

Reconstruction of fracture roughness

According to the result of spectral analysis, the power spectra of the roughness data represented negative exponential distribution. It has a pattern showing high amplitudes in low frequency domain and low amplitudes in high frequency one (Figs. 3 & 4). It means that roughness patterns of the specimens are mainly composed of components of long wavelengths.

Although spectral analysis and smoothing of spectrum were conducted, some noises are still remained in high frequency domain. The authors selected a threshold of spectrum pattern changing abruptly meaning a low pass filter. Cosine curves of each low frequency components determined by a low pass filter were overlapped resulting in reconstruction of roughness using only influential frequencies among all the components of frequencies (Fig. 5). The reconstructed roughness patterns show smooth and well matched features to the original roughness.

CONSTRUCTION OF AN AVERAGED FRACTURE AND COMPUTATION OF PERMEABILITY COEFFICIENTS

As explained in the previous sections, the Fourier transform can identify influential components among all the components of roughness. The inverse Fourier transform also reconstructs roughness feature with several influential components of roughness. In this study, a method is suggested to recognize overall geometric feature of a target fracture in a field scale based on the theory of the Fourier transform.

The six specimens used in the study were partly collected in drilled cores along a large vertical subsurface fracture in a site. The Fourier spectral analysis and noise reduction were subsequently performed on each specimen after detailed measurements of fracture roughness with the confocal laser scanning microscope. The smoothed spectra of each specimen were averaged on each frequency component (Fig. 6). Since the spectrum contains all the frequency components, it is possible to consider that the averaged spectrum shows the representative components of roughness of the target fracture. The averaged spectrum shows similar pattern of amplitudes in low frequency domain. Because the feature of the averaged spectrum is similar to that for each specimen, it indicates that the spectrum includes the overall components of each specimen. For the next step, the inverse Fourier transform was conducted to reconstruct the averaged roughness after determination of threshold of a low pass filter. The reconstructed roughness also in cludes the overall characteristics of each specimen (Fig. 7).

The meaning of this approach can be explained as follows. In general, a fracture exposed on the surface can be traced continuously, while it is impossible to

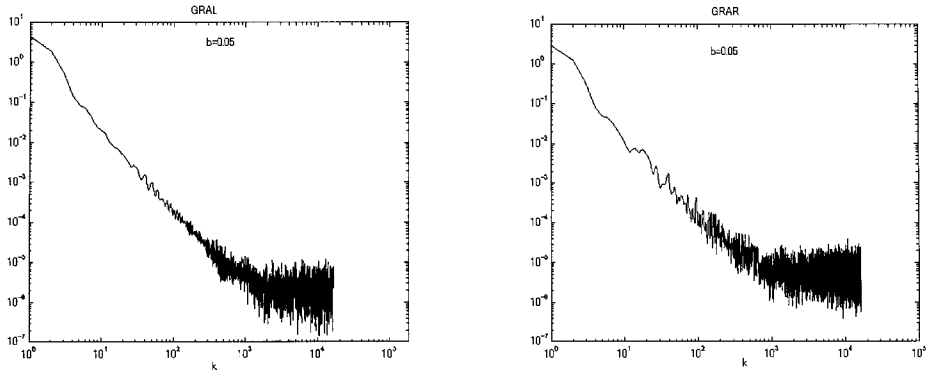

(a) GRA

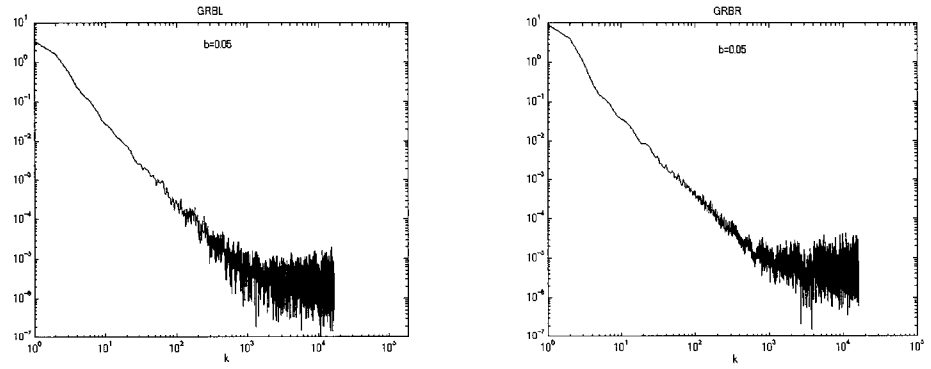

(b) GRB

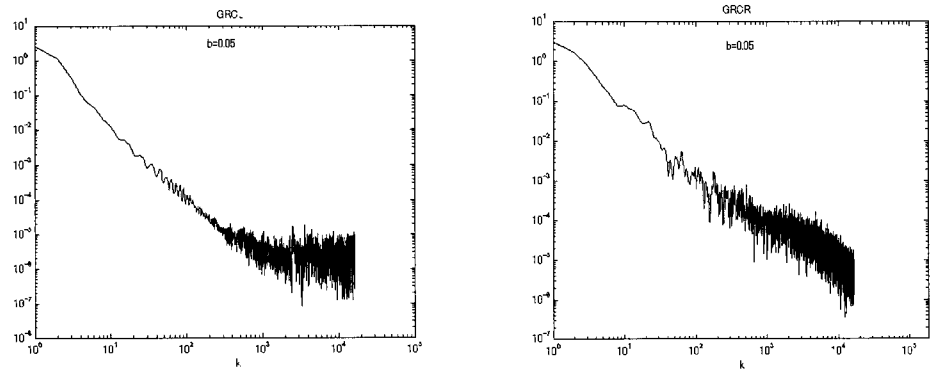

(c) GRC

Fig. 4. Result of smoothing of each spectrum using the Parzen window. 'L' of each specimen title means left part, while 'R' means right part of a specimen.

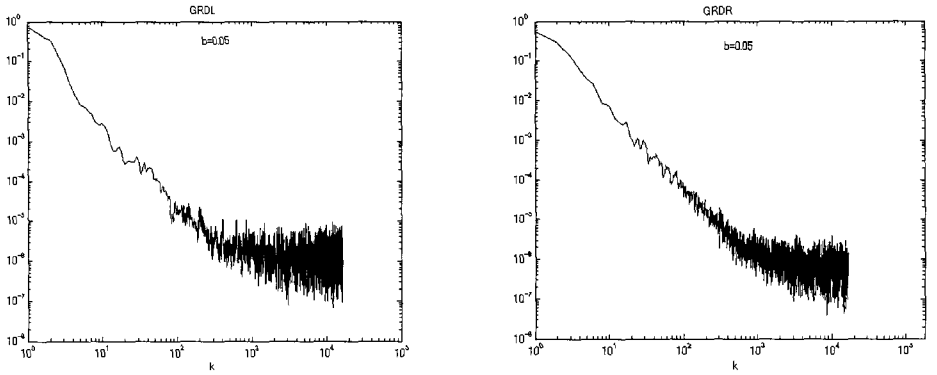

(d) GRD

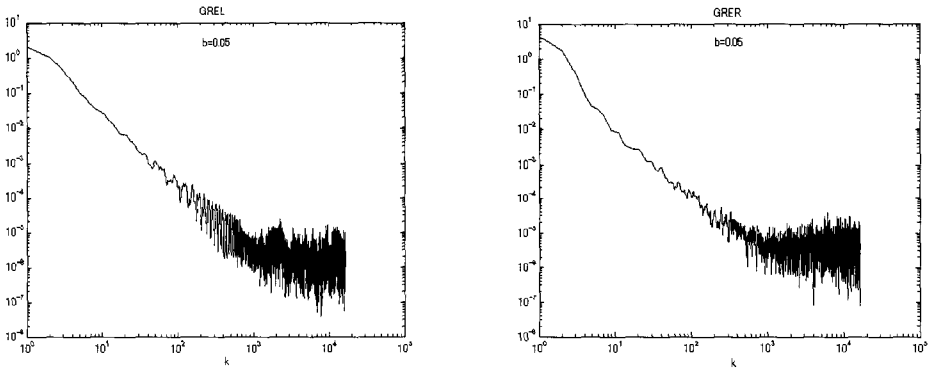

(e) GRE

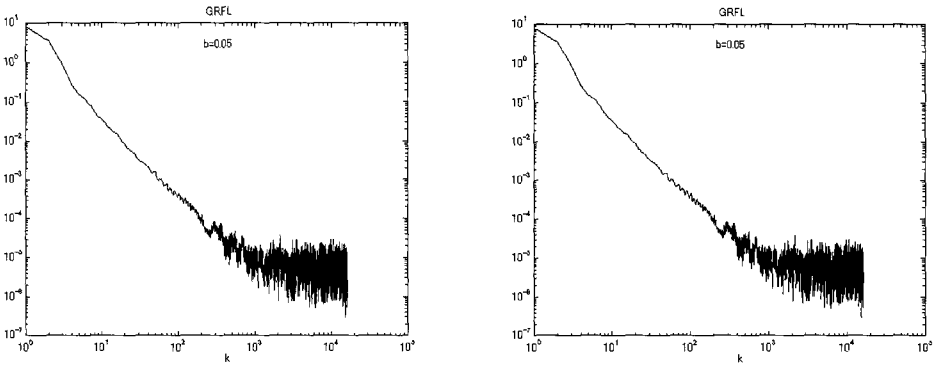

(f) GRF

Fig. 4. Continued.

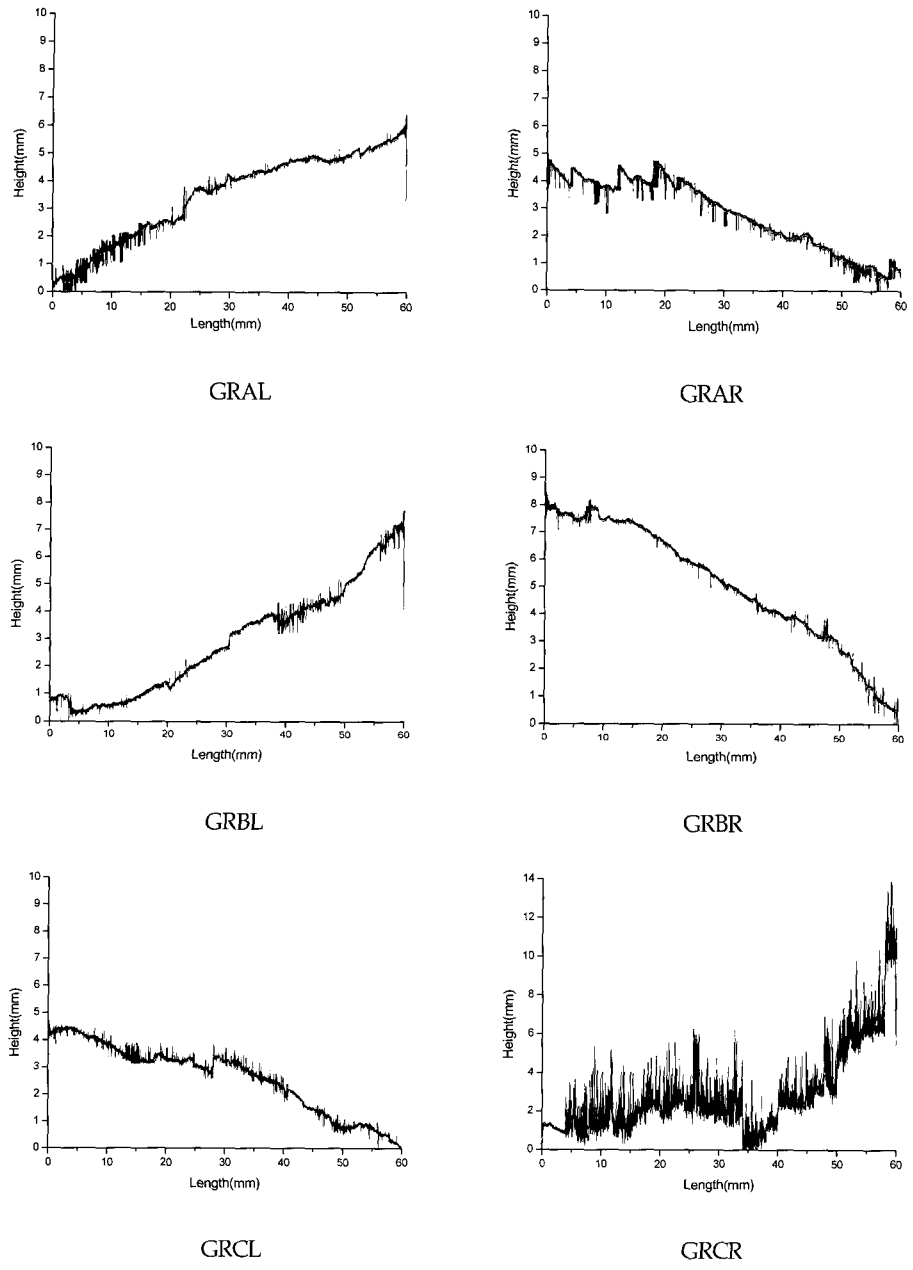

Fig. 5. Comparison of the measured roughness data of each specimen which bear noises (black) with the smoothed roughness data which were filtered by a low pass filter (red).

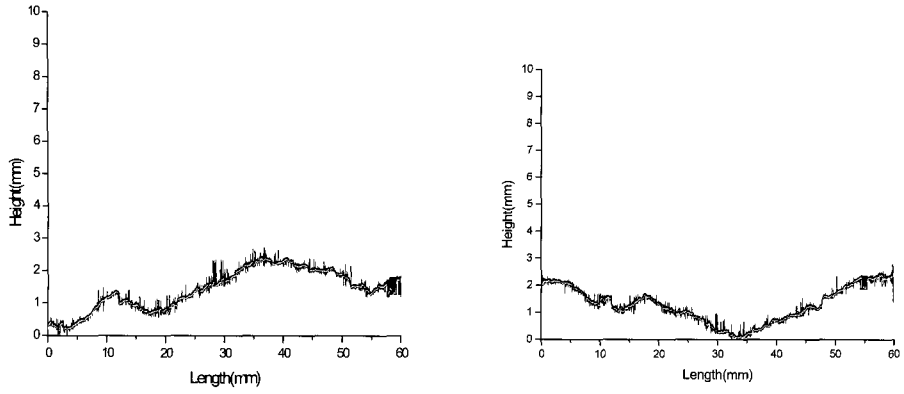

GRDL

GRDR

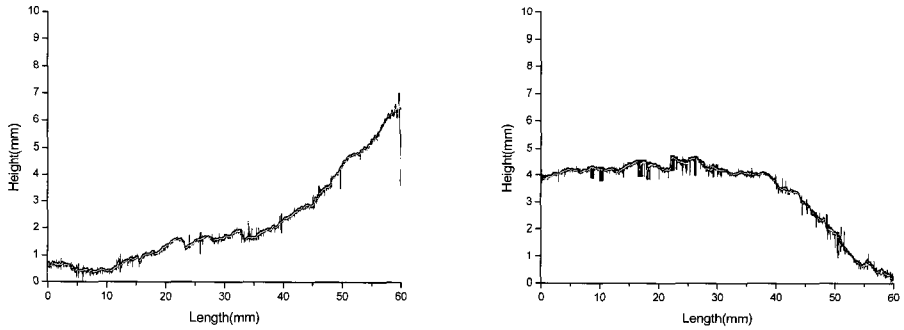

GREL

GRER

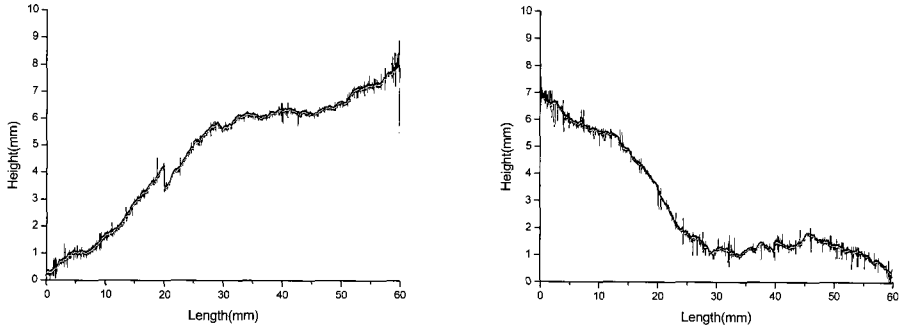

GRFL

GRFR

Fig. 5. Continued.

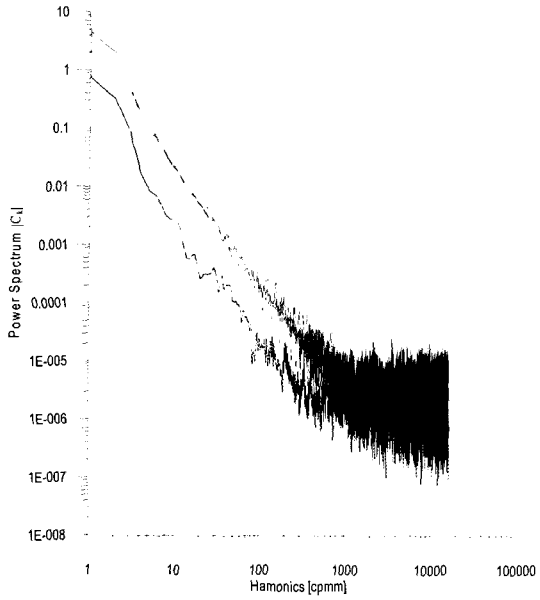

Fig. 6. The averaged spectrum acquired from the spectra of the six specimens. GRA: black; GRB: green; GRC: yellow; GRD: brown; GRE: blue; GRF: orange; Average: red.

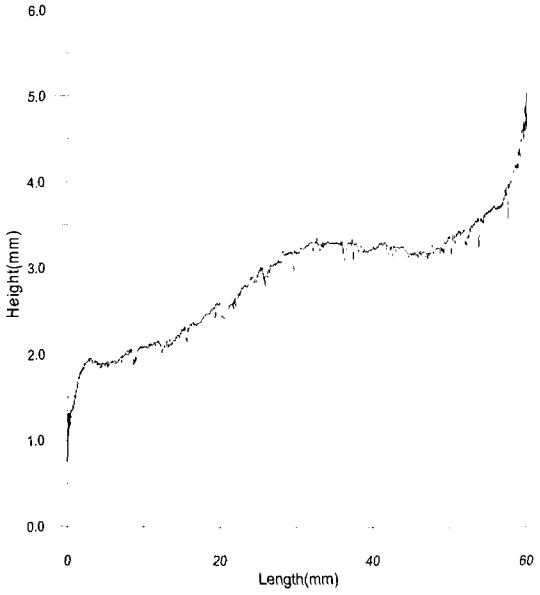

Fig. 7. Averaged roughness reconstructed by the inverse Fourier transform.

trace a fracture continuously in subsurface. Therefore, many a case have limitation to obtain reliable geometric information of a fracture which is developed in the subsurface layers. However, if it is possible to measure geometry of a target fracture with a sufficiently accurate manner in a statistical sense and to perform the spectral analysis of the geometric feature, one can understand overall geometric feature of the subsurface fracture in a large scale. The approach will be effectively applied to the analysis of permeability characteristics along a target fracture in a field scale.

After construction of several fracture models based on the reconstructed averaged roughness, the permeability coefficients were obtained under various fracture conditions by the homogenization analysis (HA). The homogenization analysis can calculate accurate permeability along a fracture with much consideration of local fracture geometry, because it calculates micro scale permeability coefficient at homogeneous microscale, and then, computes a homogenized permeability coefficient (C-permeability coefficient) at macro scale. Therefore, it is possible to analyze accurate characteristics of permeability reflected with local effect of facture geometry (Chae, 2003).

The fracture models are composed of six types such as a parallel plate model and the models that show changes of roughness patterns and aperture by five stages of shear displacement(Fig. 8). The shear displacement induced various roughness and aperture distribution. As the results of the HA computation, the C-permeability coefficients have a range between 10^{-4} and 10^{-3} cm/sec (Table 1). Compared with the C-permeability coefficients of each specimen (Table 2), the calculated results indicate that the averaged fracture models including overall geometric characteristics of each specimen are reasonable in a sense of field scale. The permeability coefficients do not follow theoretical trend of the cubic law, $Q \propto b3$, because the fracture models have rough fracture patterns (Chae et al., 2003a). In consequence, one can acquire a permeability coefficient along a fracture including overall geometric characteristics in a field scale with the above procedure.

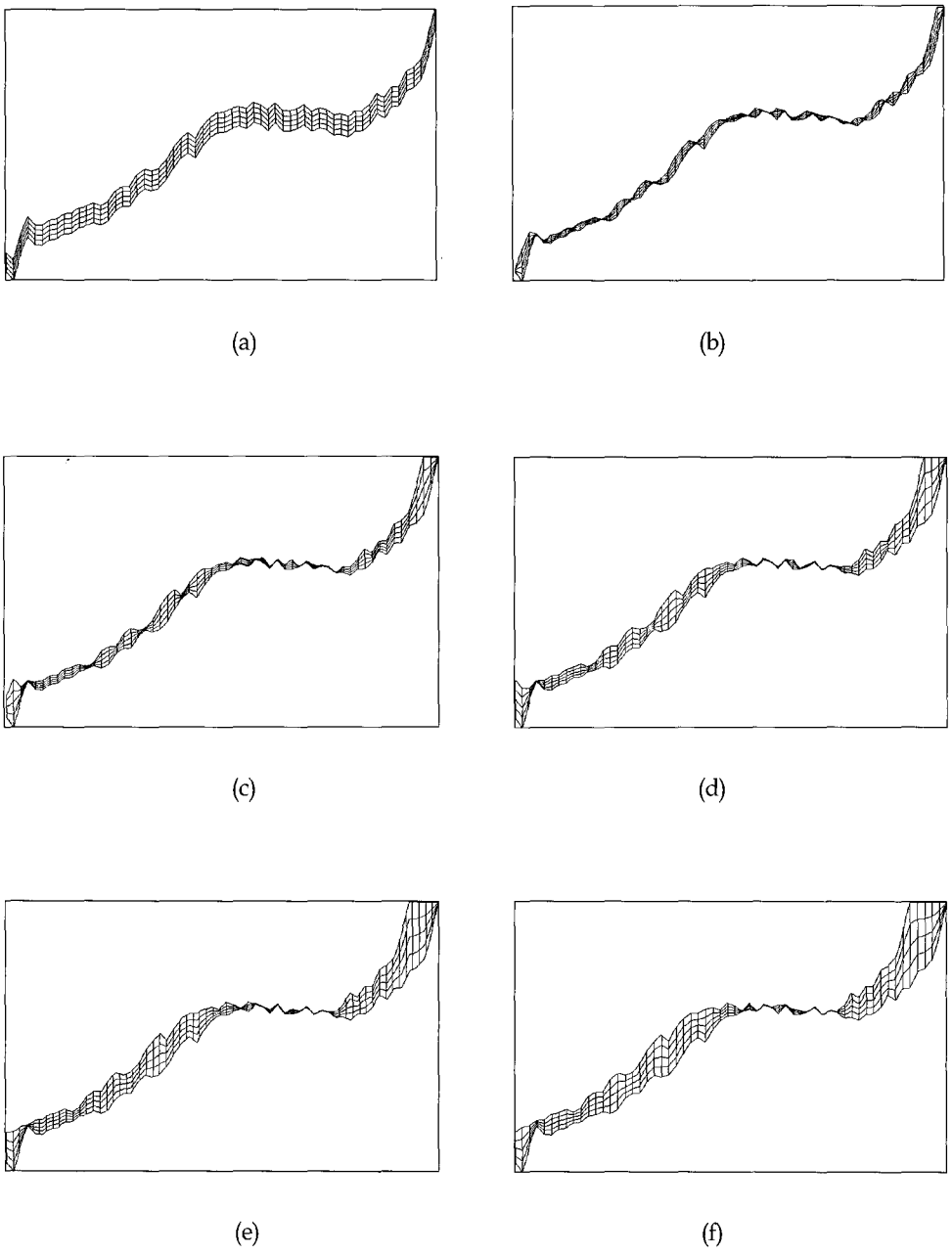

Fig. 8. Fracture models constructed based on the averaged roughness data. (a) parallel fracture walls, (b) 1mm shear displacement, (c) 2mm shear displacement, (d) 3mm shear displacement, (e) 4mm shear displacement, (f) 5mm shear displacement.

Table 1. Permeability coefficients of the averaged fracture model on the five stages of shear displacement for each specimen.

	Displacement(mm)					
	0(parallel)	1	2	3	4	5
Permeability coefficient (cm/sec)	1.47E-03	5.51E-04	1.04E-04	8.78E-04	1.14E-03	2.02E-03

Table 2. Permeability coefficients of each specimen on the five stages of shear displacement.

Shear disp. (mm)	C-permeability coefficient (cm/sec)					
	GRA	GRB	GRC	GRD	GRE	GRF
1.0	7.46E-03	1.67E-03	1.68E-01	1.43E-01	5.05E-01	5.31E-03
2.0	2.28E-03	2.00E-03	4.67E-04	4.45E-01	2.35E-02	5.31E-03
3.0	7.18E-03	7.79E-03	2.32E-04	7.60E-02	1.16E-01	4.16E-04
4.0	1.79E-02	1.79E-03	1.91E-04	1.48E-03	5.09E-02	3.22E-03
5.0	1.55E-01	1.67E-03	1.83E-04	5.94E-04	6.83E-03	1.76E-03

CONCLUSIONS

The Fourier transform analyzes complicated components of a signal into simple frequency components showing the magnitudes of the analyzed frequencies. Therefore, it is possible to identify the composition of frequency and the most effective frequency in the roughness data.

Based on the theory of the Fourier transform, this study suggests a method to recognize overall geometric feature of a target fracture in a field scale. It is possible to identify the geometric characteristics of a fracture in a large scale when sufficiently accurate measurements and the subsequent spectral analyses are performed for several fractures along the target fracture. The acquired spectra of each specimen are averaged for all the frequencies. Because the averaged spectrum includes all the frequency profiles of each specimen, the averaged spectrum shows the representative components of the fracture roughness of the target fracture. The inverse Fourier transform is conducted to reconstruct an averaged roughness after determining a threshold value of low pass filter. The reconstructed roughness feature also includes the overall geometrical characteristics of each specimen and shows a representative feature of roughness of the target subsurface fracture.

The permeability coefficients under several fracture conditions of the reconstructed averaged fracture were calculated by the homogenization analysis. The results show a range between 10^{-4} and 10^{-3} cm/sec. They indicate that the averaged

fracture models including overall geometric characteristics of each specimen are reasonable one. The approach will be effectively applied to the analysis of permeability characteristics as well as the fracture geometry in discontinuous fracture rock masses.

REFERENCES

Adler, P. M. and Thovert, J. -F., 1999, Fractures and fracture Networks, Kluwer Academic Publishers, 429.

Brown, S., Caprihan, A. and Hardy, R. 1998, Experimental observation of fluid flow channels in a single fracture, J. Geophys. Res. v. 103, n. B3, 5125 -5132.

Brown, S. R., 1995, Simple mathematical model of a rough fracture, J. Geophysical Research, v. 100, 5941-5952.

Brown, S. R., 1987, Fluid flow through rock joints: The effect of surface roughness, J. Geophysical Research, v. 92, n. B2, 1337-1347.

Brown, S. R. and Scholz, S. H., 1985, Broad bandwidth study of the topography of natural rock surfaces, J. Geophysical Research, v. 90, 12575-12582.

Chae, B. G., 2003, Characterization of hydraulic conductivity in rock fracture, Ph.D. Thesis, Nagoya Univ., Japan, 193.

Chae, B. G., Ichikawa, Y., Jeong, G. C. and Seo, Y. S., 2003a, Aperture of Granite Fracture and Effects for Fluid Flow, Materials Sci. Res. Int., v. 9, n. 4, 270-277.

Chae, B. G., Ichikawa, Y., Jeong, G. C., Seo, Y. S. and Kim, B. C., 2003b, Roughness measurement of rock discontinuities using a confocal laser scanning microscope and the Fourier spectral analysis, Engineering Geol. in press.

Develi, K., Babadagli, T. and Comlekci, C., 2001, A new computer-controlled surface-scanning device for measurement of fracture surface roughness, Computers and Geosciences, v. 27, 265-277.

Durham, W. B. and Bonner, B. P., 1993, PEAK : A new kind of surface microscope. Int. J. Rock Mech. Min. Sci. and Geomech. Abstr., v. 30, 699-702.

Gale, J., 1987, Comparison of coupled fracture deformation and fluid flow models with direct measurements of fracture pore structure and stress-flow properties, Proc. 28th U.S. Symp. Rock Mechanics, Tuscon, 1213-1222.

Gash, B., 1991, Measurement of rock properties in coal for coal bed methane production, Proceedings of the 1991 SPE (Society of Petroleum Engineers) Annual Technical Conference & Exhibition, Dallas, Texas, U.S.A. SPE #22909, 221-230.

Gentier, S. D., Billaux, D. and van Vliet, L., 1989, Laboratory testing of the voids of a fracture, Rock Mech. Rock Eng., v. 22, 149-157.

Glass, R. J., Nicholl, M. J. and Tidwell, V. C., 1995, Challenging models for flow in unsaturated, fractured rock through exploration of small scale processes, Geophys. Res. Lett. v. 22, n. 11, 1457-146033.

Hakami, E., 1992, Joint aperture measurements An experimental technique, In Proc. Int. Symp. Fractured and Jointed Rock Massses, Lake Tahoe, California, U.S.A.

Hakami, E. and Barton, N., 1990, Aperture measurements and flow experiments using transparent replicas of rock joints, In Rock Joints, Barton Stephansson (Eds), Balkema, Rotterdam, 383-390.

Hakami, E. and Stephansson, O., 1993, Experimental technique for aperture studies of intersecting joints, Proc. ISRM Int. Symp. Eurock '93, 301-308.

Huang C., White, I., Thwaite, E. G. and Bendeli, A., 1988, A non-contact laser system for measuring soil surface topography, J. Soil Sci. Soc. Am., v. 52, 350-355.

Ichikawa, Y., Kawamura, K., Uesugi, K., Seo, Y. S. and Fujii, N., 2001, Micro- and macrobehavior of granitic rock: observations and viscoelastic homogenization analysis, Comput. Methods Appl., Mech. Engrg., v. 191, 47-72.

International Society for Rock Mechanics Commission on Standardization of Laboratory and Field Tests, 1978, Int. J. Rock Mech. Min. Sci. & Geomech. Abstr., v. 15, 319-368.

Jesselle, M. W., Cox, S. J. D., Schwarze, P. and Power, W., 1995, The anisotropy of surface roughness measured using a digital photogrammetric technique, Special Pub. Geol. Soc. London, v. 92, 27-37.

Keller, K. and Bonner, B. P., 1985, Automatic, digital sys-

tem for profiling rough surfaces, Rev. Sci. Instrument, v. 56, 330-331.

Krohn, C. E. and Thompson, A. H., 1986, Fractal sandstone pores: automated measurements using scanning-electron-microscope images, Physical Review B, v. 33, 6366-6374.

Kulatilake, P. H. S. W., Shou, G., Huang, T. H. and Morgan, R. M., 1995, New peak shear strength criteria for anisotropic rock joints, Int. J. Rock Mech. Min. Sci. and Geomech. Abstr., v. 32, 673-697.

Lee, Y. H., Carr, J. R., Barr, D. J. and Haas, C. J., 1990, The fractal dimension as a measure of the roughness of rock discontinuity profiles, Int. J. Rock Mech. Min. Sci. and Geomech. Abstr., v. 27, 453-464.

Lespinasse, M. and Sausse, J., 2000, Quantification of fluid flow: hydro-mechanical behaviour of different natural rough fractures, J. Geochemical Exploration, v. 69-70, 483-486.

Maerz, N. H., Franklin, J. A. and Bennett, C. P., 1990, Joint roughness measurement using shadow profilometry, Int. J. Rock Mech. Min. Sci. and Geomech. Abstr., v. 27, 329-343.

Ohsaki, Y., 1981, Introduction to spectral analysis of seismic motion, Kajima Pub., 138-169, in Japanese.

Persoff, P. and Pruess, K., 1995, Two-phase flow visualization and relative permeability measurement in natural rough-walled rock fractures, Water Resources Res., v. 31, 1175-1186.

Plouraboue, F., Kurowski, P., Boffa, J. -M., Hulin J. -P. and Roux, S., 2000, Experimental study of the transport properties of rough self-affine fractures, J. Contaminant Hydrology, v. 46, 295-318.

Power, W. L. and Durham, W. B., 1997, Topography of natural and artificial fractures in granitic rocks: implications for studies of rock friction and fluid migration, Int. J. Rock Mech. Min. Sci., v. 34, 979-989.

Tsang, W. and Hale, F.V., 1988, A study of the application of mercury porosimetry method to a single fracture, Proc. Int. Conf. Fluid Flow in Fractured Rocks

투 고 일 2004년 1월 4일
심 사 일 2004년 1월 5일
심사완료일 2004년 2월 22일

채병곤
한국지질자원연구원 지질환경재해연구부
305-350, 대전시 유성구 가정동 30
Tel: 042-868-3052
Fax: 042-861-9723
E-mail: bgchae@kigam.re.kr